# Effects of isolated atomic collision cascades on $SiO_2$/Si interfaces studied by scanning tunneling microscopy

I. H. Wilson,* N. J. Zheng, U. Knipping, and I. S. T. Tsong
*Department of Physics, Arizona State University, Tempe, Arizona 85287*
(Received 22 February 1988; revised manuscript received 27 April 1988)

Si(100) wafers with oxide thicknesses of 40 and 200 Å were implanted with $Ge^+$ and $As^+$ ions with energies from 20 keV to 1 MeV. Low ion doses, $\sim 10^{11}$ ions/cm$^2$, were used to avoid overlap of collision cascades. The extent of cascade damage at the $SiO_2$/Si interface due to single ion impacts was examined by scanning tunneling microscopy after the oxide layer was removed by HF. The surface topography in the form of craters was found to relate to the cascade damage rather than to the removal of atoms by sputtering. There is a 1:1 correlation between the number of ion impacts and the number of craters. The crater diameter as a function of implant-ion energy agrees well with theoretical estimates of the lateral extent of the cascade due to nuclear energy deposition at the interface.

## I. INTRODUCTION

For a considerable time we have been concerned with the topography of ion-bombarded surfaces. In a recent review[1] we concluded that atomic-scale surface effects, particularly individual ion impacts, are important in nucleating surface features such as pits and asperities. Hitherto the only direct evidence of the effects of the impact of a single ion on a metal surface comes from field-ion microscopy,[2] where the vacancy structure of a near-surface depleted zone has been observed. High-resolution transmission electron microscopy (TEM) has been used to image structure changes and strain caused by collision cascades in metals[3] and semiconductors.[4] Also, high-resolution scanning electron microscopy (SEM) has been used to image 500-Å-diam pits in 100-keV $Ge^+$-bombarded Ge surfaces.[5]

We report the first attempt to determine the effects of single-ion impacts on surfaces using scanning tunneling microscopy (STM). Si(100) was chosen as the target because of the increasing importance to integrated-circuit performance, with shrinking device size, of small, ion-implantation-induced features at $SiO_2$/Si interfaces. Argon-bombarded silicon surfaces have been studied by STM previously,[6] but (as in the case of Ref. 5) high doses were used with consequent gross overlap of cascades. No model for the formation of the observed hillocks (50 Å diam $\times$ 10 Å height) was proposed. Sputtering, argon clustering, or amorphous zones were thought to be possible causal mechanisms.

In the present work we have chosen a very low ion dose ($\sim 10^{11}$ cm$^{-2}$) to avoid cascade overlap, a large range of ion energy (20 keV to 1 MeV), ions which do not form gas bubbles (As and Ge), and random and channeled implants and implantation through surface oxides of two thicknesses, 40 Å (native) and 200 Å (screen). Our objective is to observe damage induced by individual collision cascades at the oxide/silicon interface by STM in order to establish a correlation between the extent of damage and energy deposition by the incident ion.

## II. EXPERIMENT

The Ge implants were performed on a 500-keV implanter[5] at the University of Surrey using doubly charged ions for the 1-MeV implants. In this case, 2-in. wafers of Si(100) were used with a 7° tilt on an axis parallel to the wafer flat for the pseudorandom implants. Doses varied from $0.4\times10^{11}$ to $1.9\times10^{11}$ ions/cm$^2$. The As implants were performed on a commercial implanter at the Motorola Bipolar Technology Center, where 4-in. wafers (20 Ω cm, $p$ type) were used with tilt plus rotation to random orientation, and a dose of $2\times10^{11}$ ions/cm$^2$. In some cases the normal 200-Å screen oxide was removed prior to implantation.

The STM used in this work has been described elsewhere.[7] Samples ($\sim 6\times6$ mm$^2$) were etched in buffered HF for 20 min to remove the oxide layer prior to immediate transfer to the vacuum system. The time elapsed from immersion in HF to a vacuum of $\sim 10^{-5}$ torr was $\sim$15 min. STM working pressure (no bake) was $\sim 1\times10^{-7}$ torr. A new tungsten tip was used for imaging each new sample surface. Areas scanned were typically (1000 Å)$^2$, although 500- and 3000-Å scans were also used out of a maximum field of view of (6000 Å)$^2$. The tunneling current was 0.9 nA at a tip bias of $-1.7$ V.

One sample implanted with $Ge^+$ (100 keV, 7° incidence) was examined by STM in air with the native oxide intact. The tunneling current was unstable when the tip was stationary and a very noisy trace was obtained upon scanning, indicating that the tip was in contact with the oxide surface. We therefore abandoned attempts to image in air and all images reported in this work were taken in vacuum.

## III. RESULTS

A typical STM image of an unbombarded Si(100) surface is shown in Fig. 1. Irregular undulations of $\leq 10$ Å amplitude can be observed, but these are quite different in nature from bombarded craters with well-defined boun-

 

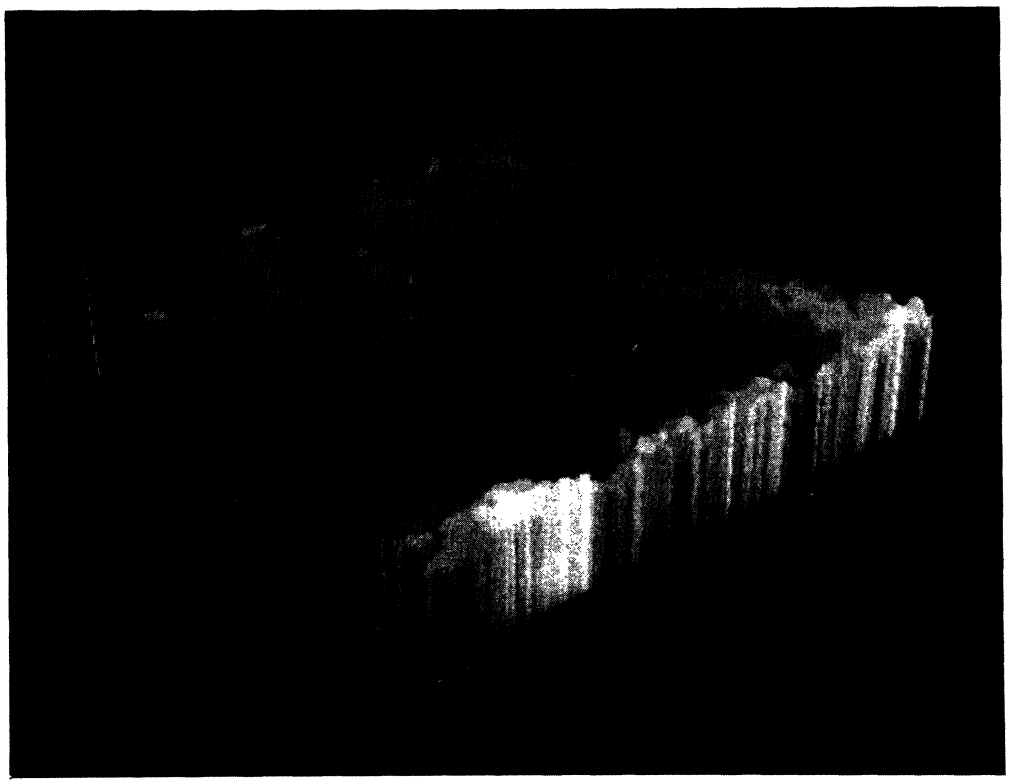

FIG. 1. Three-dimensional STM image of an unbombarded Si(100) surface. All units on the $x$-$y$-$z$ axes are in Å.

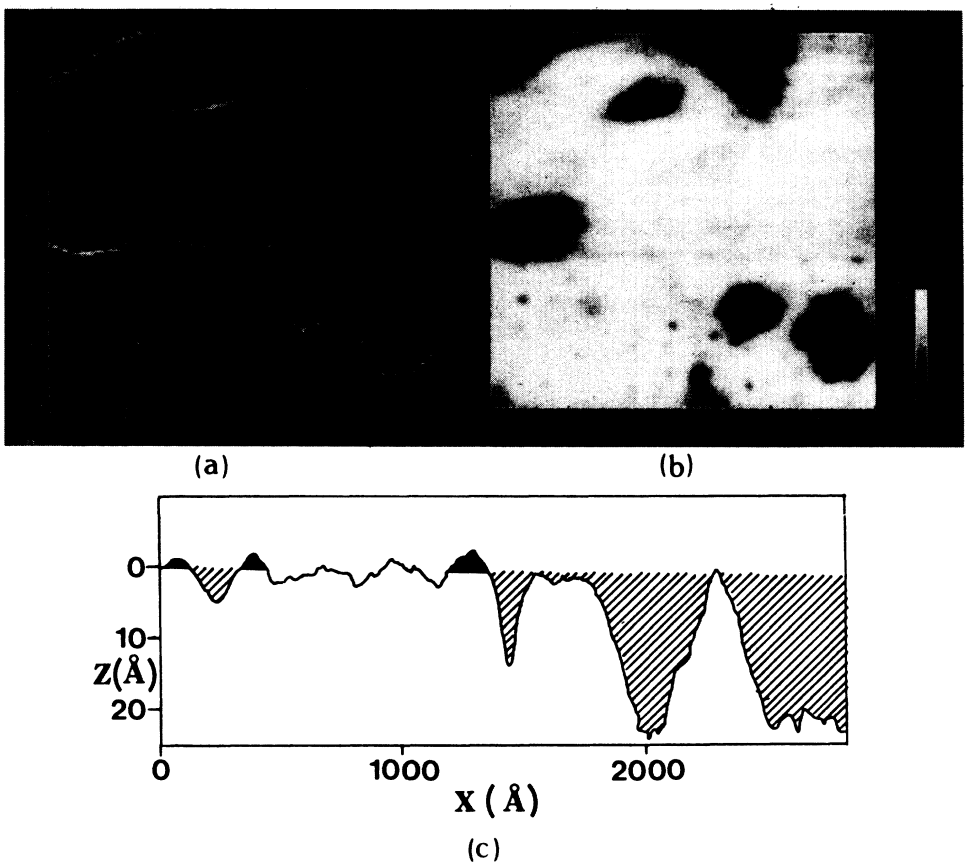


FIG. 2. (a) Line-scan and (b) gray-scale STM images of Si(100) after bombardment with 200-keV $As^+$ (200-Å screen oxide, $2\times10^{11}$ ions/cm$^2$). Scan direction is from bottom to top. (c) Single line scan from (a) with vertical ($y$) coordinate of 680 Å.

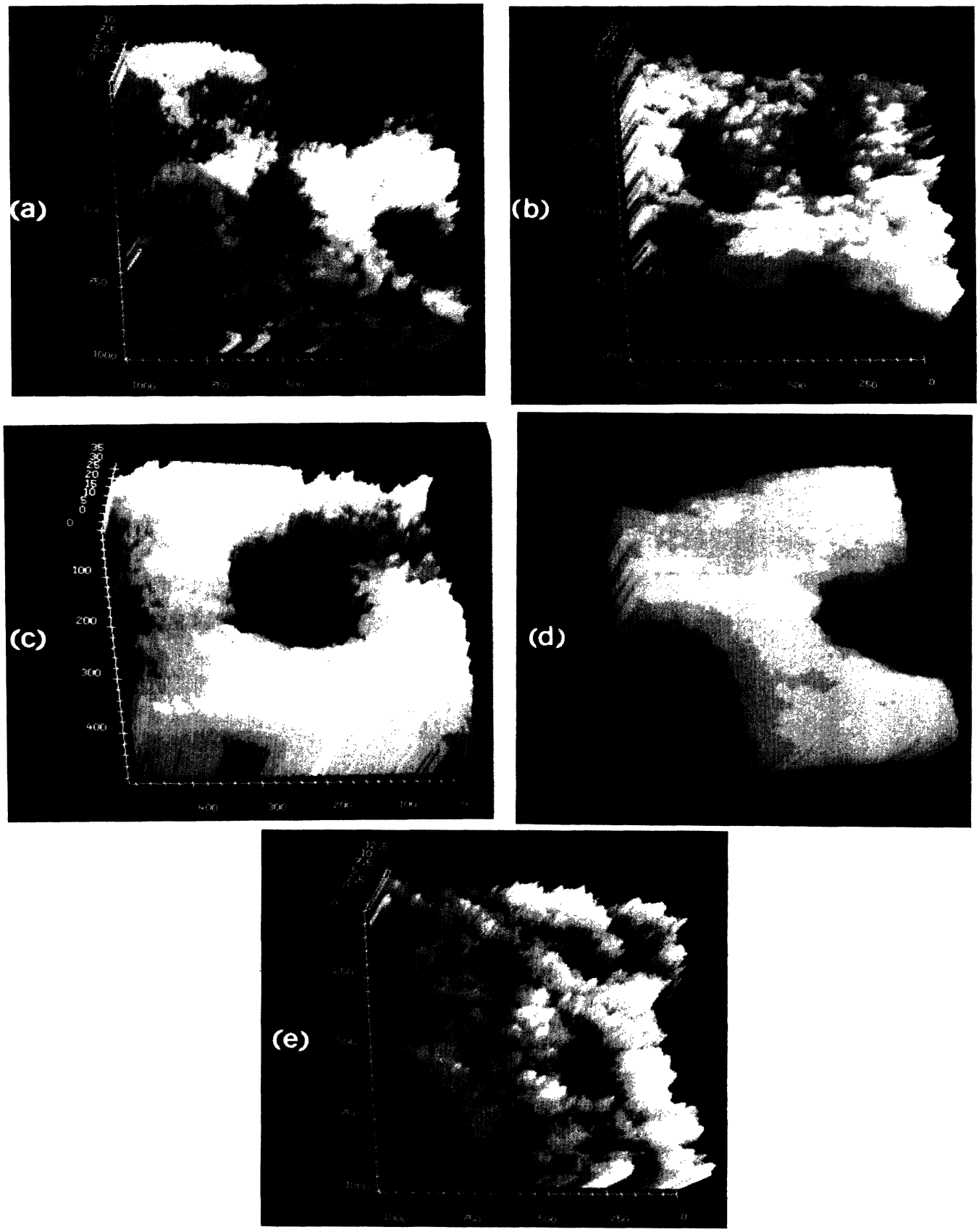


FIG. 3. Three-dimensional STM images of ion-bombarded Si(100) surfaces (40-Å native oxide, random incidence): (a) 20-keV $As^+$, (b) 50-keV $As^+$, (c) and (d) 100-keV $Ge^+$, and (e) 500-keV $Ge^+$. All units on the $x$-$y$-$z$ axes are in Å.

daries. We did not observe any regular corrugation reported by other workers at exposed $Si/SiO_2$ interfaces.[8] However, our scans were over smaller areas, so we cannot rule out the possibility of long-range regular corrugations over a larger scale. The signal trace exhibited more noise than similar line scans from a gold surface using the same STM, with random fluctuations equivalent to $\sim 2$ Å on the depth scale. We take this to be characteristic of the exposed Si surface.

On the bombarded samples, craters with diameters ranging from 20 to 800 Å and apparent depths of 3–25 Å were found. In most cases, all or part of the crater rim was raised above the surrounding surface.

Unprocessed line-scan and gray-scale images of the sample with the largest craters (200-keV $As^+$) are shown in Figs. 2(a) and 2 (b). The dark areas of the gray-scale image are craters of apparent depth 15–25 Å. Note that small ($\sim 100$ Å diam) craters can be seen in the lower part of the micrograph before a change in the tip condition, possible due to contact with the surface, leads to a degradation in resolution in the upper part. This is typical of problems encountered with large-area scans. A single line scan parallel to the $x$ axis at $y = 680$ Å is shown in Fig. 2(c). The scan intersects the center of one 150-Å-diam crater ($x$ coordinate, 1450 Å) and also the edge of one small and two large craters. Raised regions at the crater lip can be seen.

Three-dimensional plots for bombarding-ion energies of 20–to 500 keV can be seen in Fig. 3. The 1000-Å scans [panels (a), (b), and (e)] illustrate the wide range of crater diameters, while the 500-Å scans [panels (c) and (d)] show details of single large craters.

Over 1000 such craters in total were analyzed for their diameters and depths. Details of mean and standard deviation of crater diameter (typically 50–100 craters per sample) and the ratio of the number of craters to the number of ion impacts per unit area are given in Table I. The mean crater diameters are plotted as a function of incident ion energy in Fig. 4. Also plotted are theoretical estimates of the lateral extent of the 90-(eV/Å) nuclear-energy deposition contour at the interface (random incidence) with surface oxides of 40- and 200-Å thicknesses.

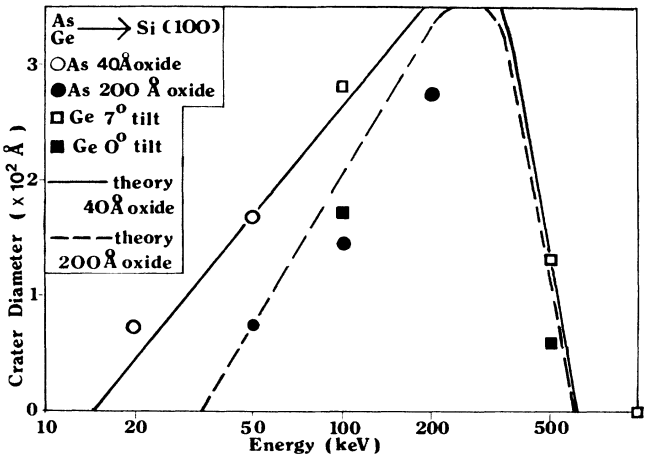


FIG. 4. Plot of the mean crater diameter vs ion energy and the theoretical prediction of the lateral extent of the cascade based on an energy-deposition cutoff at 90 eV/Å at the $SiO_2/Si$ interface for oxide thicknesses of 40 and 200 Å.

## IV. THEORETICAL ESTIMATES

The analytical implantation code PRAL (Projected Range Algorithm[9]) has recently been modified and extended to predict energy-deposition profiles.[10] The new code, called SUSPRE (Surrey University Sputter Profile, Resolution and Energy deposition), was used to determine the nuclear-energy deposition, $dE_n/dx$, as a function of depth for $As^+$ and $Ge^+$ ions on oxidized silicon (random orientation). A plot of $dE_n/dx$ versus depth is shown in Fig. 5 for the 200-Å oxide case. We wish to correlate the energy deposited laterally at the $SiO_2/Si$ interface with the observed crater diameter. The extent of

TABLE I. Experimental parameters and results. $E$ is the ion energy, $I$ the ion species, $\theta$ the ion incidence ($R$ denotes random, $A$ denotes aligned with [100]), $d_{ox}$ the oxide thickness, $D$ the mean crater diameter, $\sigma$ the standard deviation of the crater diameter, $n/\phi$ the ratio of the number of craters to the number of ion impacts per unit area, and $d_m$ the maximum apparent crater depth.

| $E$ (keV) | $I$ | $\theta$ | $d_{ox}$ (Å) | $D$ (Å) | $\sigma$ (Å) | $\sigma/D$ | $n/\phi$ | $d_m$ (Å) | $d_m/D$ |
|---|---|---|---|---|---|---|---|---|---|
| 20 | As | $R$ | 40 | 73 | 52 | 0.71 | 1.05 | 9 | 0.12 |
| 50 | As | $R$ | 40 | 169 | 95 | 0.56 | 0.95 | 10 | 0.06 |
| 50 | As | $R$ | 200 | 76 | 34 | 0.45 | 1.30 | 3.5 | 0.05 |
| 100 | As | $R$ | 200 | 144 | 57 | 0.40 | 1.05 | 5 | 0.04 |
| 200 | As | $R$ | 200 | 275 | 158 | 0.57 | 0.85 | 25 | 0.09 |
| 100 | Ge | $R$ | 40 | 283 | 104 | 0.37 | 0.89 | 20 | 0.07 |
| 500 | Ge | $R$ | 40 | 134 | 71 | 0.53 | 1.85 | 15 | 0.11 |
| 1000 | Ge | $R$ | 40 | | | | | | |
| 100 | Ge | $A$ | 40 | 172 | 60 | 0.35 | 1.15 | 8 | 0.05 |
| 500 | Ge | $A$ | 40 | 58 | 30 | 0.52 | 4.69 | 12 | 0.21 |
| 1000 | Ge | $A$ | 40 | | | | | | |

lateral energy deposition can be estimated from the depth distribution shown in Fig. 5 by determining the difference between two depths in Si: one where $dE_n/dx$ falls to a value $(dE_n/dx)_I$ just below the interface, and one at a cutoff value $(dE_n/dx)_c$. The implication is that $(dE_n/dx)_c$ is the limit of damage effects, i.e., damage is negligible below this value. We find that the value of $(dE_n/dx)_c$ that best fits the experimental results is 90 eV/Å. As an example, we show in Fig. 5 that for an incident-ion ($As^+$ or $Ge^+$) energy of 200 keV, the difference in depths at $(dE_n/dn)_I = 135$ eV/Å (for a 200-Å-thick oxide) and $(dE_n/dx)_c = 90$ eV/Å is 320 Å, which agrees reasonably well with the mean crater diameter for 200-keV $As^+$ ions listed in Table I. Figure 6 illustrates schematically the mean contours of constant energy deposition and the formation of a crater within the 90-(eV/Å) contour at the interface for an incident ion of several hundred keV. The plot in Fig. 4 shows reasonable agreement between crater diameters and theoretical estimates of the lateral extent of the cascade (i.e., nuclear-energy deposition) at the interface.

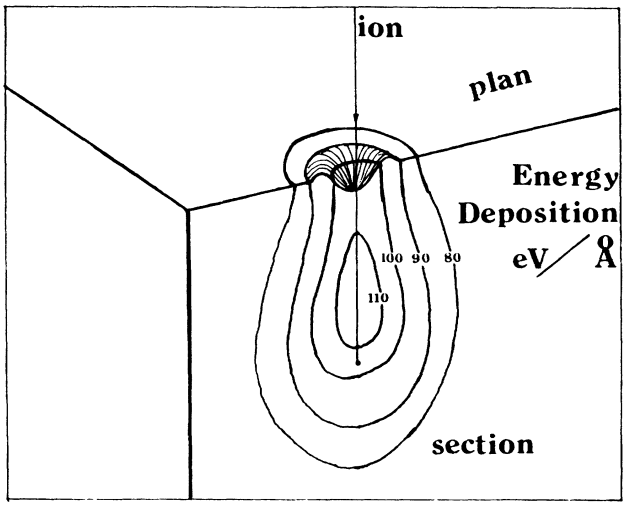


FIG. 6. Schematic illustration of energy-deposition contours at the $SiO_2/Si$ interface for an incident ion of several hundred keV showing a crater inside the 90-(eV/Å) contour.

## V. DISCUSSION

From Fig. 4 we can see the following.

(i) The experimental results are a good fit to the estimated nuclear-energy deposition.

(ii) Channeled implants yield significantly smaller crater diameters.

(iii) There is no significant difference between the $Ge^+$ and $As^+$ implants. This is expected due to their similar masses.

From Table I we see the following.

(i) Within experimental error there is a 1:1 correlation between the number of ion impacts and the number of craters, except for 500 keV, where the number of craters exceeds the number of ion impacts.

(ii) The apparent maximum crater depth $d_m$ is smaller for the lower-energy implants (50 and 100 keV) with a screen oxide (200 Å). The ratio of depth to diameter is greatest at the extremes of the energy range where the mean crater diameter is small.

(iii) The standard deviation of crater diameter, $\sigma$, is larger than the counting error ($\sim 0.1$) ranging from 0.35 to 0.56, except for the lowest energy, where a larger value of 0.71 was recorded.

A few craters were found in the case of the 1-MeV implants, but the numbers were too small to be statistically significant, partly due to the low dose used ($0.4\times10^{11}$ ions/cm$^2$) in order to avoid cascade overlap.

The results are consistent with the formation of craters at the $SiO_2/Si$ interface by displacement damage in individual atomic-collision cascades. The following observations support this.

(i) Mean crater diameters $D$ for random ion incidence are correlated with estimated values of $(dE_n/dx)_I$.

(ii) Mean crater diameters for channeled implants are considerably smaller than those for random implants at the same energy, as would be expected from lower values of $(dE_n/dx)_I$.

(iii) The number density of craters is the same as the number density of ion impacts. The exception is the 500-keV case. It is known from TEM studies[4] that multiple heavily damaged regions are formed in one cascade at high energies. It appears that this occurs for the 500-keV implants.

(iv) The large standard deviation $\sigma$ in crater diameter reflects the statistical nature of cascade formation.

One point of comparison with TEM measurements is for 20-keV $As^+$ (Ref. 4) [although Si(111) was used in this case]. In the TEM work, transverse (i.e., parallel to the

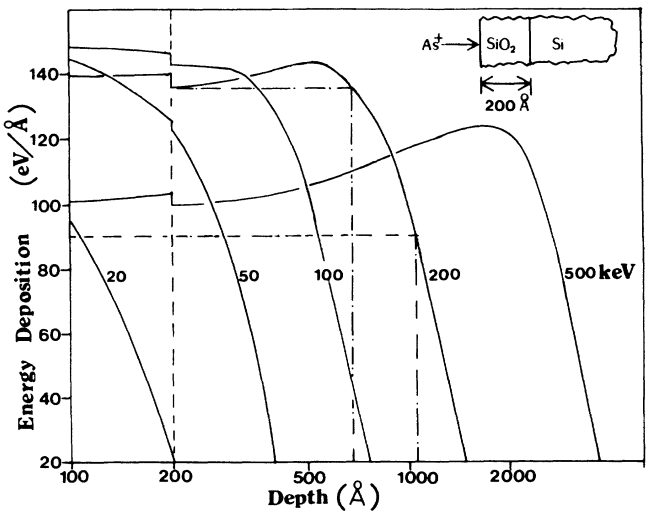


FIG. 5. Stopping of $As^+$ primary ions (20–500 keV) in Si with a 200-Å oxide shown as a plot of nuclear-energy deposition vs depth calculated by SUSPRE (Ref. 10). The dashed line indicates the $SiO_2/Si$ interface. The dashed-dotted lines indicate $(dE_n/dx)_I$ and $(dE_n/dx)_c$ and their difference in depths of 320 Å for 200-keV incident energy.

surface) straggling, $\langle \gamma^2 \rangle^{1/2}$, was predicted to be 68 Å by Monte Carlo simulation and 89 Å by WSS theory.[11] Our simple estimate from SUSPRE predicts, for the 40-Å oxide case, a lateral extent of energy deposition of 45 Å at the interface. TEM observation of regions of strong structure contrast (indicative of heavily defective regions) gave a mean diameter, $D_{\text{TEM}} = 30$ Å, while our STM mean crater diameter was 73 Å. Our measured crater diameter is very similar to the calculated $\langle \gamma^2 \rangle^{1/2}$, while the TEM images appear less sensitive to damage, although it was found that the ratio $D_{\text{TEM}} / \langle \gamma^2 \rangle^{1/2}$ increases above unity for dense cascades.

The main unanswered question is the means of formation of the craters. There are three possibilities.

(1) The reactivity of silicon is increased by radiation damage in the form of atomic displacements. If the craters were formed by an enhanced etch rate during oxide removal by HF, then one would expect a strong dependence of crater depth on ion energy. Such a dependence is not observed, though one must note here that the true depth may be masked by the STM tip effects.

(2) The targets with screen oxides (200-Å thickness) exhibited shallower craters. The Ge-implanted samples, which were stored much longer between implant and analysis, exhibited deeper craters. Possibly the damaged region near the interface reacts slowly with oxygen diffusing from the ambient. Growth of the extra oxide will be limited by the supply of oxygen from the oxide and ambient. However, estimated oxidation rates at room temperature are too low to account for the observed effects.

(3) We feel that more plausible explanation of this phenomenon, which would account for the raised crater rim, comes from the point-defect distribution in the cascade. The center of the cascade is rich in vacancies, the periphery is rich in interstitials. In the atomic rearrangements following the cascade, vacancy clusters will collapse to form dislocations loops and interstitials will condense as extra planes. It seems from our results that the stresses arising from these processes result in sinking and raising of the surface, respectively, so the crater profile results from the asymmetry in the point-defect distribution close to the surface. We show in Fig. 7 a schematic illustration of crater formation due to a single energetic ion. The crater volume is consistent with the number of displacements, but it is difficult to quantify since only the region of the ion track just below the surface will be effective. If the bulk of the damage is deeply buried, the stress due to the vacancy-rich core will be canceled out by that due to the interstitial-rich shell.

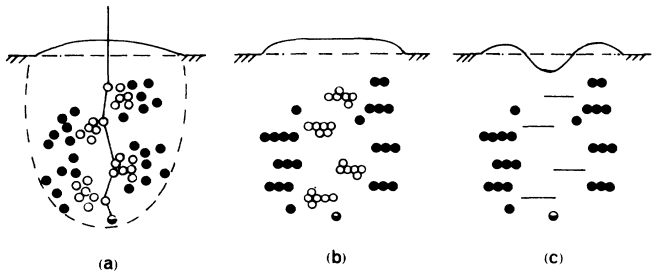


FIG. 7. Schematic illustration showing (a) creation of vacancies and interstitials by an incoming ion, (b) formation of vacancy clusters and interstitial planes, and (c) collapse of the surface to fill in the vacancies forming a crater and raising of the crater periphery due to the extra planes. ○, vacancy; ●, interstitial; and ◒ implanted ion.

STM studies of ion impact on surfaces provide useful data on the statistics of cascade formation for comparison with computer simulations and other experimental techniques. It can be inferred from our results that craters on a nanometer scale caused by defect clustering in individual cascades is a major precursor of surface roughening during ion bombardment. This roughening may well be the cause of the dramatic improvement in thin-film adhesion reported for low-dose, high-energy ion bombardment.[12]

## VI. CONCLUSIONS

We have studied the effects of atomic-collision cascades at $SiO_2/Si$ interfaces caused by single-ion impacts in the energy range 20 keV to 1 MeV. The major topographic effect is the formation of craters. The crater diameters at the interface were measured by STM after the oxide was etched away by HF. The mean crater diameters as a function of implant-ion energy agree well with theoretical calculations of the lateral extent of the cascade due to nuclear-energy deposition at the $SiO_2/Si$ interface assuming a cutoff $(dE_n/dx)_c$ value of 90 eV/Å.

## ACKNOWLEDGMENTS

We thank T. C. Smith (Motorola) for performing implantation of silicon wafers and Roger Webb (University of Surrey) for supplying the latest version of SUSPRE.

*On leave from the University of Surrey, Guildford, U.K.

[1] I. H. Wilson, in *Materials Modification by High-Fluence Ion Beams,* Proceedings of the NATO Advanced Study Institute, Lisbon, 1987, edited by R. Kelly (Plenum, New York, 1987).

[2] D. N. Seidman, M. I. Current, D. Pramanik, and C. Y. Wei, Nucl. Instrum. Methods **182/183**, 477 (1981), and references therein.

[3] W. Jager and K. L. Merkle in Proceedings of the 9th International Congress on Electron Microscopy, Toronto, 1978 (unpublished); see also K. L. Merkle and W. Jager, Philos. Mag. A **44**, 741 (1981).

[4] L. M. Howe and M. H. Rainville, Nucl. Instrum. Methods B **19/20**, 61 (1987).

[5] I. H. Wilson, J. Appl. Phys. **53**, 1698 (1982).

[6] R. M. Feenstra and G. S. Oehrlein, J. Vac. Sci. Technol. B **3**, 1136 (1985); Appl. Phys. Lett. **47**, 97 (1985).

[7] M. J. Zheng, U. Knipping, I. S. T. Tsong, W. T. Petuskey, and J. C. Barry, J. Vac. Sci. Technol. A **6**, 457 (1988).

[8]M. S. Khaikin, A. M. Troyanovskii, V. S. Edelman, U. M. Pudalov, and S. G. Semenchinskii, Pis'ma Zh. Eksp. Teor. Fiz. **44**, 193 (1986) [JETP. Lett. **44**, 245 (1986)].

[9]J. P. Biersak, Nucl. Instrum. Methods **182/183**, 199 (1981).

[10]R. P. Webb and I. H. Wilson, in *Proceedings of the 2nd International Conference on Simulation of Semiconductor Devices and Processes,* edited by K. Board and D. R. J. Owen (Pineridge, Swansea, UK, 1986), p. 249.

[11]K. B. Winterbon, P. Sigmund, and J. B. Sanders, K. Dan. Vidensk Selsk. Mat.-Fys. Medd. **37**, No. 14 (1970).

[12]J. E. Griffith, Y. Qiu, and T. A. Tombrello, Nucl. Instrum. Methods **198**, 607 (1982).

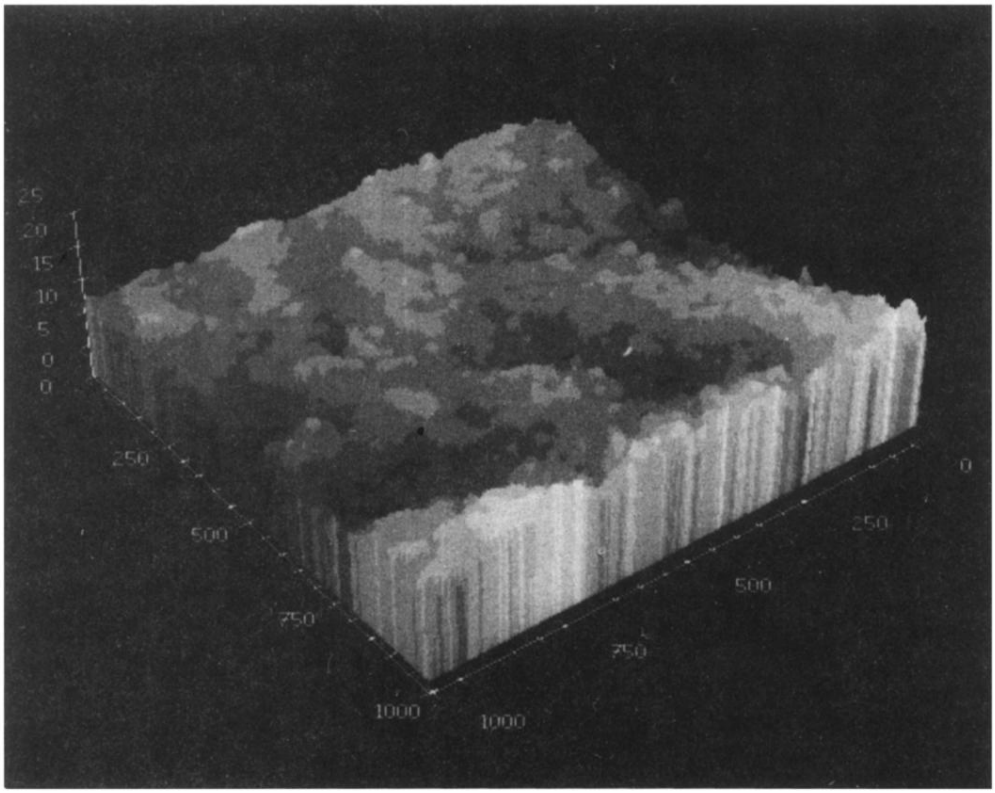


FIG. 1. Three-dimensional STM image of an unbombarded Si(100) surface. All units on the $x$-$y$-$z$ axes are in Å.

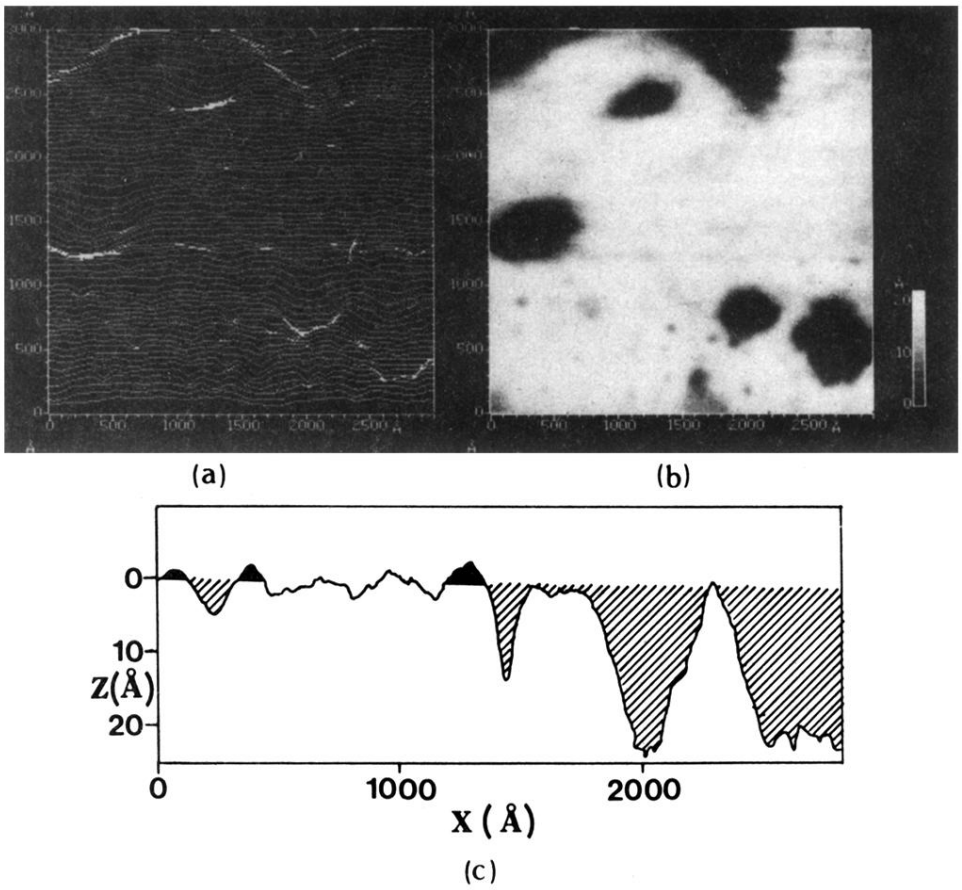


FIG. 2. (a) Line-scan and (b) gray-scale STM images of Si(100) after bombardment with 200-keV $As^+$ (200-Å screen oxide, $2\times10^{11}$ ions/cm$^2$). Scan direction is from bottom to top. (c) Single line scan from (a) with vertical ($y$) coordinate of 680 Å.

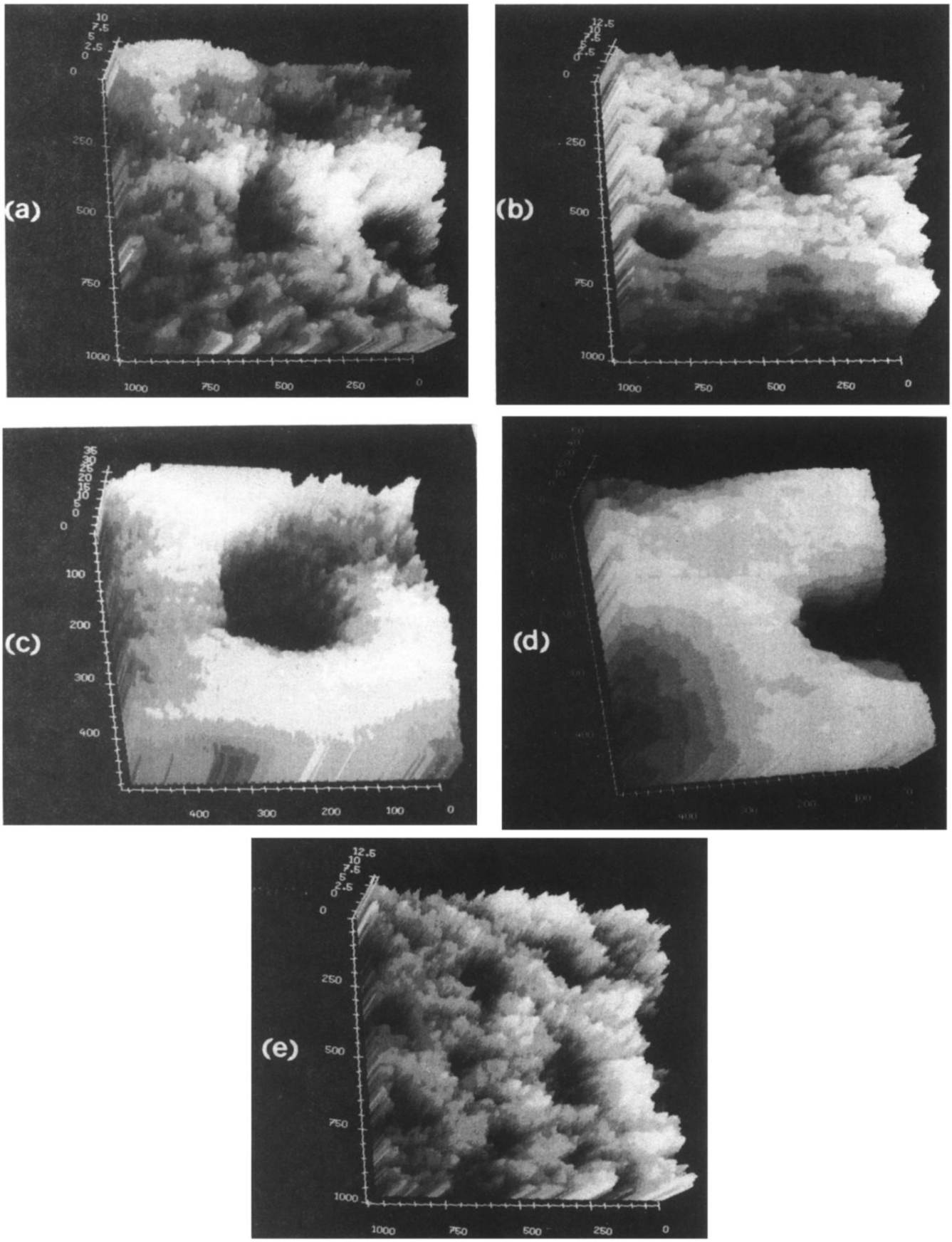


FIG. 3. Three-dimensional STM images of ion-bombarded Si(100) surfaces (40-Å native oxide, random incidence): (a) 20-keV $As^+$, (b) 50-keV $As^+$, (c) and (d) 100-keV $Ge^+$, and (e) 500-keV $Ge^+$. All units on the $x$-$y$-$z$ axes are in Å.